[Patrick Oßwald, Julia Zinsmeister, Trupti Kathrotia, Maíra Alves-Fortunato, Victor Burger, Rina van der Westhuizen, Carl Viljoen, Kalle Lehto, Reetu Sallinen, Kati Sandberg, Manfred Aigner, Patrick Le Clercq, Markus Köhler, Combustion Kinetics of Alternative Jet Fuels, Part-I: Experimental Flow Reactor Study, 302 (2021) 120735]

The original publication is available at www.elsevier.com

https://doi.org/10.1016/j.fuel.2021.120735

Combustion Kinetics of Alternative Jet Fuels, Part-I: Experimental Flow Reactor Study

Authors: Patrick Oßwald[1*], Julia Zinsmeister[1], Trupti Kathrotia[1], Maíra Alves-Fortunato[2], Victor Burger[3], Rina van der Westhuizen[3], Carl Viljoen[3], Kalle Lehto[4], Reetu Sallinen[4], Kati Sandberg[4], Manfred Aigner[1], Patrick Le Clercq[1], Markus Köhler[1]

[1] Institute of Combustion Technology, German Aerospace Center (DLR), 70569 Stuttgart, Germany
[2] IFP Energies Nouvelles (IFPEN), 1 et 4 avenue de Bois-Préau, 92852 Rueil-Malmaison, Cedex, France
[3] Sasol Energy, 1 Klasie Havenga Road, Sasolburg 1947, South Africa
[4] Neste Corporation, Keilaranta 21, 02150 Espoo, Finland

* Corresponding Author: Patrick Oßwald,
German Aerospace Center, Pfaffenwaldring 38-40, 70569 Stuttgart, Germany
phone: +49-711-6862-265 ; email: patrick.osswald@dlr.de

Abstract

A comprehensive collection of technical aviation fuels enabled an experimental and numerical study on detailed combustion chemistry and pollutant formation presented in a series of 3 interlinking parts. Part-I: Experimental Flow Reactor Study focuses on the characterization of 42 technical jet fuels and provides experimental speciation data for model development presented in Part-II: Model and Surrogate Strategy. Model validation based on the presented technical fuels here is presented in Part-III: Model Application on Technical Jet Fuels.

The fuels investigated in this study cover a broad range of approved SAFs (Sustainable Aviation Fuels), candidates for approval, and technical products outside the present ASTM-D7566 specification and is completed by reference fuels (ASTM-D1655). This includes SAF components such as HEFA (Hydroprocessed Esters and Fatty Acids), ATJ (Alcohol-To-Jet), SIP (Synthesized Iso-Paraffins), and Fischer-Tropsch-products as well as their blends.

A systematic investigation of the soot precursor chemistry by analyzing the influence of the complex chemical fuel composition on the intermediate species pool is presented. The experimental set-up consists of an atmospheric flow reactor with coupled molecular-beam mass spectrometer (MBMS).

Quantitative evolution of combustion reaction intermediates is recorded for fuel-rich (Φ=1.2) and fuel-lean (Φ=0.8) conditions at intermediate temperatures up to 1200K including small intermediate species (e.g. ethylene, butene) and soot precursor species (e.g. benzene, naphthalene, phenanthrene).

A general systematic dependency of the soot precursor concentration on the degree of unsaturation (Index of Hydrogen Deficiency) or the hydrogen content, respectively, is demonstrated. Furthermore, larger soot precursor concentrations depend on the naphthalene content of the fuel.

Keywords

Technical Jet Fuels, Synthetic Fuels, Speciation, Soot Precursor, Laminar Flow Reactor, Combustion Kinetics

1. Introduction

High requirements regarding safety together with weight limitation and long lifetime of aircraft make aviation one of the most difficult sectors to decarbonize. The industry relies on synthesized carbon neutral fuels (SAF: Sustainable Aviation Fuel) to achieve their climate goals. Even though alternative technologies such as electric- or hydrogen-powered aircraft are envisaged as long-term perspectives, there is no other option available for long-distance flights in the mid-term. Consequently, several pathways for producing carbon-neutral aviation fuels from renewable feedstocks are currently investigated [1-3].

The specification for synthetic turbine fuels (ASTM-D7566) allows blending up to 50vol% of synthetic components to conventional crude oil-based fuel (ASTM-D1655). In particular specification of new synthetic routes is a highly dynamic field. By the end of 2020 seven synthetic blend-stocks have been annexed to the ASTM-D7566-20b: a) Synthesized Paraffinic Kerosene (SPK), produced by Fischer-Tropsch (FT) synthesis from various feedstocks, b) Hydroprocessed Esters and Fatty Acids (HEFA) gained from mono-, di-, and triglycerides, free fatty acids or fatty acid methyl esters, c) Synthesized Iso-Paraffins (SIP) produced from hydroprocessed fermented sugars via biotechnological processes. SIP is currently limited to 10vol% blending fraction. d) Synthesized Paraffinic Kerosene plus Aromatics (SPK/A) are FT-Paraffins with addition of nonpetroleum alkylated light aromatics. e) Alcohol-To-Jet Synthetic Paraffinic Kerosene (ATJ-SPK) produced by dehydration, oligomerization and hydrogenation from biotechnologically accessible alcohols (currently isobutanol and ethanol), f) Catalytic Hydrothermolysis Jet (CHJ) fuel based on a hydrothermal conversion and hydrotreating operations of fats, oils and grease feedstocks, and g) Hydroprocessed Hydrocarbons, Esters and Fatty Acids (HC-HEFAs) that incorporate biomass from specific sources, to date from algae (Botryococcus braunii). HC-HEFA is also limited to 10vol%. In addition, Sasol's Semi- and Fully-Synthetic Jet Fuel (SSJF and FSJF) from the Secunda plant in South Africa is annexed to the UK MoD DEF-STAN 91-091 specification as well as to ASTM-D1655.

While carbon dioxide emission savings primarily depend on the feedstock of the SAF production, many have shown their ability to reduce the particulate emission of various aero-engines in ground and flight tests e.g. [4-6]. This is of particular interest when non-CO_2 climate effects like contrail formation [7] or local airport air quality are considered [8]. These effects are typically assigned to the reduction of the aromatic content [9] of the fuel when blended with aromatic-free synthetic components. More recent experiments indicate the fuel's hydrogen content being a better parameter to predict the soot emission of a fuel than the aromatic content [5, 10, 11].

With the implementation of alternative fuels, the need of chemical kinetic models for correct prediction of the aforementioned fuel effects is increasing [12]. A successful approach is presented with the HyChem model developed at Stanford University [13, 14]. However, when combustion kinetics is considered, the complexity of technical fuels, that typically contain several hundreds of individual chemical species, needs to be reduced to a proper surrogate of a few chemical species [15, 16]. Reaction kinetics of the surrogate molecules is consequently developed based on experimental datasets for the neat substances. Fundamental chemical kinetics experiments on real fuels are scare and often limited to global parameters such as ignition delay time e.g. [15, 17] and laminar flame speed e.g. [18]. For these global parameters jet fuels complying with the ASTM specification do not show distinct differences [19].

Resolving species evolution for complex fuels is a challenging task. Investigations are typically bounded to a limited set of technical fuels. Dagaut and coworkers [20] have performed a noticeable number of speciation experiments in a jet-stirred-reactor for technical fuels e.g. Gas-To-Liquid SPK [21]. Data are also available from Princeton's variable pressure flow reactor [22] or shock-tube species-time history measurements [14]. To the best of our knowledge no systematic investigation of a larger number of technical fuels has been performed on a speciation level. With high regards to the famous answer to the ultimate question for life, universe, and everything in Douglas Adam's "The Hitchhiker's Guide to the Galaxy" – 42 – we present a dataset on this number of aviation fuels in Part-I. This collection was measured under comparable boundary conditions at the DLR high-

106 temperature flow reactor [23] with coupled molecular-beam mass spectrometry (MBMS) for
107 quantitative speciation of the occurring combustion intermediates.

108 2. Fuels

109 The 42 fuels investigated in this study cover a broad range of approved SAFs, blend stocks,
110 candidates for approval, and technical products outside the present ASTM-D7566 specification. The
111 set is completed by reference fuels (ASTM-D1655), covering a wide range of crude-based jet fuels.
112 The fuels have been acquired within different international projects, which provide additional data
113 ranging from generic test rig and burner results up to full size aero-engine measurements. Fuels are
114 shortly described and linked to their projects and additional data available.

115 The Fischer-Tropsch (FT) fuels investigated within the framework of the DLR project "Emission
116 and Climate Impact of Alternative Fuels" (ECLIF) include the FSJF as well as three different blends
117 of Semi-Synthetic Jet Fuels (SSJF1-3) provided by the South African FT-specialist SASOL. For
118 these certified fuels, ground [10] and in-flight [7] exhaust gas measurements have been performed in
119 the plume of the IAE V2527-A5 engines of DLR's A320 Advanced Technology Research Aircraft
120 (DLR-ATRA). The choice of FT-Fuels is completed by six product streams also provided by SASOL
121 and a crude FT-product ("FT-Light") from a Power-to-Liquid source [24] extending the database
122 beyond the limitations of the ASTM specification.

123 Hydroprocessed Esters and Fatty Acids (HEFA) are represented by the fuels used in NASA-DLRs
124 ACCESS2 (Alternative Fuel Effects on Contrails and Cruise Emissions Study) campaign [6, 25],
125 namely a 50:50 blend of low sulfur Jet A and HEFA-SPK fuel. Ground and flight measurement
126 results are available for the CFM56-2-C1 NASA DC-8 aircraft [6]. Three further HEFA (Paramount
127 Refinery) blends have been studied within the joint "NASA/DLR-Multidisciplinary Airborne
128 eXperiments" (ND-MAX) or ECLIF2 campaign, where ground and flight measurements with the
129 DLR-ATRA have been performed. Due to the renewable feedstock the fuels are called "Sustainable
130 Alternative Jet Fuel" (SAJF1-3). These approved fuel blends have been accompanied by two blends
131 and a neat High Freezing Point (HFP) HEFA product currently tested by Neste for aviation purposes.
132 Another bio-derived jet fuel investigated here is ARA catalytic hydrothermolysis (CHJ) fuel

(ReadiJet^{TM}) obtained from an engine (CFM56-5-C4) exhaust measurement campaign (airegEM) at an engine test facility [26]. This fuel also fulfills the ASTM specification parameters and was approved recently. Due to the feedstock we have grouped the CHJ fuel with the HEFA fuels.

As a third class, fuels involving biotechnological fermentation of sugar or starch are included. Among the approved fuels of this group are ATJ and SIP. SIP consists almost exclusively (98%) of a single molecule: Farnesane (2,6,10-Trimethyldodecane, $C_{15}H_{32}$) [27, 28]. The ATJ investigated in this study also primarily consist of a limited number of molecules: 2,2,4,6,6-pentamethyl heptane $C_{12}H_{26}$ (75%) and 2,2,4,4,6,8,8-heptamethyl nonane $C_{16}H_{34}$ (16%) the remainder are other highly branched C7-C22 isoparaffins. The neat ATJ was also used for emissions measurement on a CFM56-5C4 engine [26] at a test rig. Additionally, we have completed the list by looking at ATJ-SKA [29], which contains an adequate fraction of aromatics to fulfill the final blend specification requirements. Approval of this fuel type is ongoing.

Finally, we have investigated approved fuel blends containing multiple alternative components. Within the German national framework of "DEMO-SPK" [30] a so-called multiblend (MB) containing HEFA and ATJ was used for emissions measurement on an A300-600F (Pratt&Whitney PW4158 engine). Moreover, a multiblend containing additional SIP (MB SIP) was investigated also herein.

For comparison 13 conventional crude-based jet fuels were investigated. These include the reference fuels used in the above mentioned projects: ECLIF [10], ECLIF2/ND-MAX, ACCESS2 [6], airegEM [26] and DEMO-SPK [30]. Additionally the fuels POSF-10264 (A1), POSF-10325 (A2) and POSF-10289 (A3) were gathered from the US consortium "National Jet Fuel Combustion Program" (NJFCP) [31]. Within the EU-H2020 project JETSCREEN an additional Jet A-1 fuel (JS-A1) and it's severely hydrotreated (JS-A1.3) version have been measured alongside with high naphthalene containing fuel surrogates (JS-C1 and C3).

ASTM-D7566 specifies 24 properties to be achieved for the final blend. Additional properties are required for the alternative blending component including specific production pathways. In the

following we consider the D7566 requirement for fuels/blends labeled as “on-spec”. Table 1 summarizes the investigated fuels, their grouping as used within the present work and respective literature references. Selected key properties are summarized in Tab. 2.

Table 1: Summary of fuel naming and grouping.

#	Fuel	Long name	Group	Reference
1	E1-Ref1	ECLIF Ref 1	Fossil	[10]
2	E1-Ref2	ECLIF Ref 2	Fossil	[10]
3	E1-SSJF1	ECLIF SSJF 1	FT	[10]
4	E1-SSJF2	ECLIF SSJF 2	FT	[10]
5	E1-SSFJ3	ECLIF SSJF 3	FT	[10]
6	E1-FSJF	ECLIF FSJF	FT	[10]
7	S-IPK	SASOL IPK	FT	-
8	S-IPK-A	SASOL IPK-A	FT	-
9	S-HN1	SASOL Heavy Naphtha #1	FT	-
10	S-HN2	SASOL Heavy Naphtha #2	FT	-
11	S-LD1	SASOL Light Distillate #1	FT	-
12	S-LD2	SASOL Light Distillate #2	FT	-
13	E2-Ref3	ECLIF2/ND-MAX Ref 3	Fossil	-
14	E2-Ref4	ECLIF2/ND-MAX Ref 4	Fossil	-
15	E2-SAJF1	ECLIF2/ND-MAX SAJF 1	HEFA	-
16	E2-SAJF2	ECLIF2/ND-MAX SAJF 2	HEFA	-
17	E2-SAJF3	ECLIF2/ND-MAX SAJF 3	HEFA	-
18	JS-B2	ECLIF2/ND-MAX HEFA	HEFA	-
19	aEM-Ref	airegEM Ref	Fossil	[26]
20	JS-B3	airegEM ReadiJet™	HEFA	[26]
21	JS-B1	airegEM ATJ	Alc./Sug.	[26]
22	ATJ-SKA	ATJ-SKA	Alc./Sug.	[29]
23	SIP	SIP (Farnesane)	Alc./Sug.	[29]
24	FT-Light	FT-Light	FT	[24]
25	D-Ref-A/C	DEMO-SPK Ref A/C	Fossil	[30]
26	D-Ref-Lab	DEMO-SPK Ref Lab	Fossil	[32]
27	D-MB-A/C	DEMO-SPK MB A/C	HEFA	[30]
28	D-MB-SIP	DEMO-SPK MB SIP	HEFA	[30]
29	JS-A1	JETSCREEN JS-A1	Fossil	[33]
30	JS-A1.3	JETSCREEN JS-A1.3	Fossil	[33]
31	JS-B1	JETSCREEN JS-B1	Alc./Sug.	[33]
32	JS-C1	JETSCREEN JS-C1	-	[33]
33	JS-C3	JETSCREEN JS-C3	-	[33]
34	NJFCP-A1	NJFCP A1 (JP-8 POSF 10264)	Fossil	[31]
35	NJFCP-A2	NJFCP A2 (Jet-A POSF 10325)	Fossil	[31]
36	NJFCP-A3	NJFCP A3 (JP-5 POSF 10289)	Fossil	[31]
37	Acc-Ref	ACCESS2 Reference	Fossil	[6]
38	Acc-HEFA50	ACCESS2 HEFA Blend (50:50)	HEFA	[6]
39	N-Ref	Neste Jet A-1 Ref	Fossil	-
40	N-HFP-B1	Neste HFP HEFA Blend 1	HEFA	-
41	N-HFP-B2	Neste HFP HEFA Blend 2	HEFA	-
42	N-NeatHFP	Neste HFP HEFA Neat	HEFA	-

164 **Table 2**: Summary of selected fuel properties.

Fuel	wH (NMR)[a] [mass-%]	IHD[b] [-]	wNa[c] [mass-%]	M (L&K)[d] [g/mol]	wH (GCxGC) [mass-%]	M (GCxGC) [g/mol]	n/iso-Par. ratio [-]	n-Paraffins [mass-%]	iso-Paraffins [mass-%]	Mono-cyclic Paraffins [mass-%]	Bicyclic Paraffins [mass-%]	Poly-cyclic Paraffins [mass-%]	Mono-cyclic Aromatics [mass-%]	Naph-theno-Aromatics [mass-%]	Bicyclic Aromatics [mass-%]	GCxGC Source
E1-Ref1	13.67	1.460	1.78	166	13.9	155	0.947	22.2	23.4	23.2	9.3	1.5	13.5	4.5	2.4	[e]
E1-Ref2	13.73	1.451	2.29	165	13.9	155	1.171	25.4	21.7	22.6	8.8	1.3	13.3	3.7	3.2	[e]
E1-SSJF1	14.36	0.851	1.04	162	14.5	158	0.259	14.0	54.0	14.5	5.2	0.8	7.8	2.4	1.4	[e]
E1-SSJF2	14.53	0.763	0.99	156	14.6	156	0.193	11.8	61.0	11.8	4.4	0.4	7.5	1.7	1.4	[e]
E1-SSFJ3	14.01	1.277	1.52	164	14.1	156	0.625	20.2	32.3	20.5	7.9	1.3	11.7	4.0	2.1	[e]
E1-FSJF	14.17	1.113	0.30	159	14.3	160	0.074	3.7	49.7	13.1	16.4	7.7	3.7	5.4	0.2	[e]
S-IPK	15.34	0.048	0.01	149	15.4	158	0.000	0.0	95.2	4.8	0.0	0.0	0.0	0.0	0.0	[e]
S-IPK-A	14.31	1.022	0.01	150	14.3	156	0.031	2.2	68.7	7.2	1.0	0.0	20.4	0.6	0.0	[e]
S-HN1	14.79	0.616	0.02	147	14.8	140	1.453	45.4	31.2	9.5	5.7	0.0	5.0	3.1	0.0	[e]
S-HN2	12.57	2.367	0.40	139	12.6	130	2.107	22.6	10.7	12.3	9.4	0.0	35.0	9.7	0.3	[e]
S-LD1	14.01	1.240	0.27	176	14.1	166	1.046	31.7	30.3	12.6	2.1	0.1	16.3	6.4	0.2	[e]
S-LD2	12.87	2.379	0.67	179	12.9	167	1.946	5.5	2.8	17.6	38.9	15.3	4.5	14.8	0.5	[e]
E2-Ref3	13.65	1.624	1.67	165	13.7	152	0.760	15.3	20.1	28.6	13.5	0.7	12.3	7.6	2.0	[e]
E2-Ref4	14.08	1.251	0.11	152	14.1	143	0.917	22.1	24.1	28.0	7.5	0.1	14.2	4.0	0.2	[e]
E2-SAJF1	14.40	0.903	0.86	169	14.5	156	0.344	16.8	48.8	14.9	7.2	0.3	6.7	4.1	1.1	[e]
E2-SAJF2	14.51	0.891	0.06	156	14.5	146	0.560	22.4	40.1	20.3	4.4	0.1	9.9	2.7	0.1	[e]
E2-SAJF3	14.04	1.255	0.92	162	14.1	150	0.591	18.3	31.0	24.0	9.2	0.4	10.7	5.4	1.1	[e]
JS-B2	15.37	0.022	0.01	172	15.4	166	0.205	16.8	81.8	1.2	0.1	0.0	0.1	0.0	0.0	[e]
aEM-Ref	13.98	1.374	1.66	165	n/a	n/a	n/a	n/a	n/a	n/a	n/a	n/a	n/a	n/a	n/a	n/a
JS-B3	13.60	1.834	0.22	165	13.5	159	1.864	17.5	9.4	30.6	17.3	0.0	14.4	10.5	0.3	[f]
JS-B1	15.31	0.001	0.00	160	15.3	180	0.000	0.0	99.9	0.1	0.0	0.0	0.0	0.0	0.0	[f]
ATJ-SKA	14.61	0.780	0.04	163	n/a	n/a	n/a	n/a	n/a	n/a	n/a	n/a	n/a	n/a	n/a	n/a
SIP	15.09	0.000	0.00	204	15.2	212	0.000	n/a	n/a	n/a	n/a	n/a	n/a	n/a	n/a	n/a
FT-Light	15.12	0.266	0.01	152	15.2	140	60.377	71.5	1.2	23.8	0.0	0.0	0.0	0.0	0.0	[24]
D-Ref-A/C	13.79	1.535	0.33	158	n/a	n/a	n/a	n/a	n/a	n/a	n/a	n/a	n/a	n/a	n/a	n/a
D-Ref-Lab	13.93	1.424	0.28	165	n/a	n/a	n/a	n/a	n/a	n/a	n/a	n/a	n/a	n/a	n/a	n/a
D-MB-A/C	14.32	1.049	0.25	160	n/a	n/a	n/a	n/a	n/a	n/a	n/a	n/a	n/a	n/a	n/a	n/a

Fuel	wH (NMR)[a] [mass-%]	IHD[b] [-]	wNa[c] [mass-%]	M (L&K)[d] [g/mol]	wH (GCxGC) [mass-%]	M (GCxGC) [g/mol]	n/iso-Par. ratio [-]	n-Paraffins [mass-%]	iso-Paraffins [mass-%]	Mono-cyclic Paraffins [mass-%]	Bicyclic Paraffins [mass-%]	Poly-cyclic Paraffins [mass-%]	Mono-cyclic Aromatics [mass-%]	Naph-theno-Aromatics [mass-%]	Bicyclic Aromatics [mass-%]	GCxGC Source
D-MB-SIP	14.14	1.225	0.23	166	n/a	n/a	n/a	n/a	n/a	n/a	n/a	n/a	n/a	n/a	n/a	n/a
JS-A1	14.02	1.341	1.36	156	14.0	150	0.625	19.2	30.7	21.8	8.0	0.0	15.5	2.9	1.8	[f]
JS-A1.3	14.43	0.886	0.03	156	14.5	150	0.622	20.6	33.1	26.5	10.7	0.0	8.0	1.0	0.0	[f]
JS-B1	15.31	0.001	0.00	155	15.3	180	0.000	0.0	99.9	0.1	0.0	0.0	0.0	0.0	0.0	[f]
JS-C1	12.66	2.859	14.58	190	12.6	182	0.673	10.1	15.0	16.4	25.7	8.1	1.9	2.9	19.9	[f]
JS-C3	13.68	1.781	4.72	195	n/a	n/a	n/a	n/a	n/a	n/a	n/a	n/a	n/a	n/a	n/a	n/a
NJFCP-A1	14.37	0.923	0.86	159	14.5	152	0.676	26.9	39.7	17.0	3.0	0.1	10.9	1.5	1.1	[31]
NJFCP-A2	13.90	1.363	2.12	168	14.0	159	0.680	20.1	29.5	24.9	6.8	0.2	12.9	3.4	2.3	[31]
NJFCP-A3	13.56	1.746	1.06	175	13.6	166	0.766	13.9	18.2	31.4	16.0	0.1	10.4	8.9	1.3	[31]
Acc-Ref	13.70	1.656	0.94	168	n/a	n/a	n/a	n/a	n/a	n/a	n/a	n/a	n/a	n/a	n/a	n/a
Acc-HEFA50	14.42	0.948	0.48	172	n/a	n/a	n/a	n/a	n/a	n/a	n/a	n/a	n/a	n/a	n/a	n/a
N-Ref	13.99	1.325	0.56	147	n/a	n/a	n/a	n/a	n/a	n/a	n/a	n/a	n/a	n/a	n/a	n/a
N-HFP-B1	14.16	1.184	0.45	151	n/a	n/a	n/a	n/a	n/a	n/a	n/a	n/a	n/a	n/a	n/a	n/a
N-HFP-B2	14.31	1.059	0.40	160	n/a	n/a	n/a	n/a	n/a	n/a	n/a	n/a	n/a	n/a	n/a	n/a
N-NeatHFP	15.04	0.090	0.03	235	n/a	n/a	n/a	n/a	n/a	n/a	n/a	n/a	n/a	n/a	n/a	n/a

[a] Hydrogen content measured according to ASTM-D7171
[b] Index of Hydrogen Deficiency calculated according to Eq.1
[c] Naphthalene content measured according to ASTM-D1840, Limit of quantification LoQ=0.1mass-%
[d] Lee Kesler [34] correlation between T50, density and molar mass
[e] GCxGC-Source: Sasol Energy, South Africa
[f] GCxGC-Source: IFP Energies Nouvelles (IFPEN), France

3. Experiment

The experimental approach follows previous studies [35-38]. Thus only a brief description is presented here with more details available in [23] including a detailed description of the experimental set-up and data evaluation. A schematic drawing is given in Fig. 1.

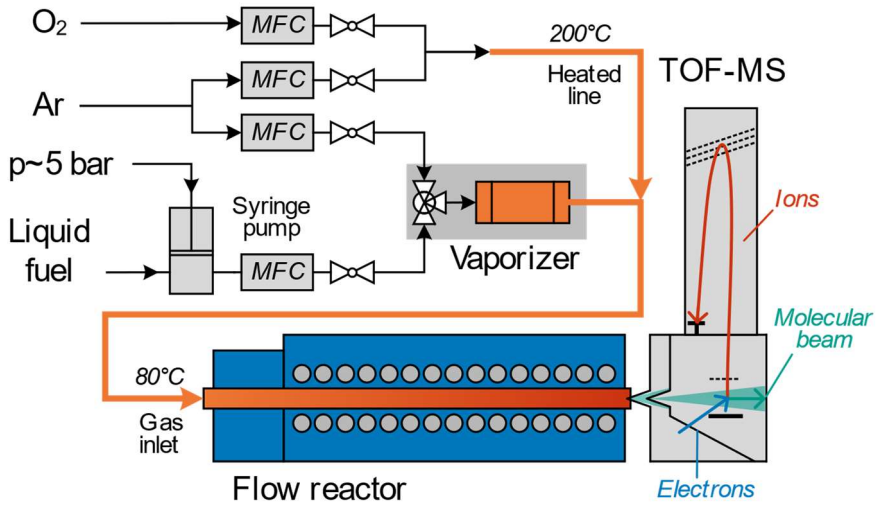

Figure 1: Experimental set-up: Flow reactor with time-of-flight mass spectrometer (TOF-MS) and gas supply including Coriolis mass flow controller (MFC).

The DLR high-temperature flow reactor consists of a reactor including gas supply, and the coupled molecular beam mass spectrometry (MBMS) system for detection of the reaction intermediates. The reactor (40mm diameter, 1000mm heated length) is placed in a high-temperature oven operating at ambient pressure (~980mbar). Highly diluted reactants (oxygen, pre-vaporized fuel, 99% Ar) are fed to the reactor at moderate temperatures (80°C). Mass flows are controlled using Coriolis flow meters for high precision, particularly useful for the chemically complex technical fuel mixture. The fuel is completely evaporated (Bronkhorst CEM) and supplied slightly heated into the reactor. Complete evaporation is ensured (and controlled regularly) by the low fuel fraction requiring only a low vapor pressure.

All measurements are designed to keep the carbon and diluent flow constant throughout the experiments. For all fuels, slightly rich (Φ=1.2) and lean (Φ=0.8) conditions are achieved by adding the respective amounts of oxygen which may consequently lead to slightly differed total volume

flow. The resulting difference in residence time is, however, negligible due to the high dilution. Inlet conditions are summarized in Table 3. Stoichiometry Φ is calculated from the NMR (ASTM-D7171) results for Hydrogen content. Heteroatoms are neglected. Measurements are performed by applying a constant-rate decreasing temperature ramp (-200K/h) covering the full range of complete oxidation to the unburnt reactants (typically 750-1200 K). Resulting residence times are in the range of 2s depending on the respective oven temperature.

Chemical species exiting the reactor are quantitatively monitored with the MBMS system by quenching the reaction immediately through rapid expansion into a molecular beam. The molecular beam is guided through the electron ionization (EI) ion source of the TOF mass spectrometer, which is capable of resolving the elemental composition (C/H/O) of the occurring stable and reactive combustion intermediates. Soft ionization conditions (10.5eV, actual value) are applied to avoid fragmentation of the species at the ion source.

Major species (reactants and products) are recorded in parallel by a quadrupole MS operating at high ionization energies (70eV) for optimal sensitivity. Within the quadrupole measurements the m/z 57 signal is recorded and used as average fuel signal. This signal refers to most hydrocarbon species especially those of aliphatic nature and was used to calculate an average “fuel” profile.

Data reduction follows established procedures [23, 37]. Combustion intermediates are calibrated using cold gas samples of known concentration with a few exceptions where estimation of the respective ionization cross section based on the RICS method (Relative Ionization Cross Section [23, 39]) was applied. The complex chemical nature of the technical fuels is accounted by calibrating the fuel compounds according to the detailed GCxGC analysis of the respective fuel when available (compare Tab. 2). The detailed composition, i.e. mass fractions by chemical class and carbon number, of the fuels is given in the electronic supplement when available.

The experimental uncertainty of the determined mole fractions is typically within ±20% for direct calibrated species. Due to the soft ionization, chemical structures of the combustion intermediates are not resolved and always the sum of isomers is measured. Since individual isomers exhibit

individual ionization cross sections, the uncertainty may be significantly higher, when several isomers occur. Calibration is always based on a single isomer chosen on the basis of experiences from isomer resolving experiments, e.g. [40, 41]. However, the reproducibility of the experiment is excellent and relative comparisons between the fuels can be performed with high accuracy. The neat ATJ fuel (same batch) for instance was measured twice (within the projects JETSCREEN “JS-B1” and airegEM “ATJ”) by different operators within a time span of about two years. Both measurements are reported herein and exhibit excellent agreement even though experimental conditions differ slightly. Results presented herein are available as electronic supplement, however, additional species profiles are available from the authors upon request.

Table 3: Inlet flow conditions for the individual measurements. Stoichiometry Φ is calculated from the NMR (ASTM-D7171) results for Hydrogen content. Heteroatoms are neglected.

	Ar	Fuel	O_2 (Fuel-rich)		O_2 (Fuel-lean)	
Fuel	[g/min]	[mg/min]	[mg/min]	Φ	[mg/min]	Φ
ECLIF Ref 1	17.64	31.1	88.1	1.19	132.1	0.80
ECLIF Ref 2	17.64	31.1	88.1	1.20	132.1	0.80
ECLIF SSJF 1	17.64	31.4	89.7	1.20	134.5	0.80
ECLIF SSJF 2	17.64	31.4	89.9	1.20	134.8	0.80
ECLIF SSJF 3	17.64	31.2	88.5	1.20	132.8	0.80
ECLIF FSJF	17.64	31.3	88.9	1.20	133.4	0.80
SASOL IPK	17.64	31.67	91.77	1.20	137.65	0.80
SASOL IPK-A	17.64	31.3	89.2	1.20	133.8	0.80
SASOL Heavy Naphtha #1	17.64	31.5	90.4	1.20	135.6	0.80
SASOL Heavy Naphtha #2	17.64	30.7	84.94	1.20	127.4	0.80
SASOL Light Distillate #1	17.64	31.1	88.6	1.19	132.9	0.80
SASOL Light Distillate #2	17.64	30.78	85.83	1.20	128.74	0.80
ECLIF2/ND-MAX Ref 3	17.64	31.02	87.5	1.20	131.2	0.80
ECLIF2/ND-MAX Ref 4	17.64	31.19	88.6	1.20	132.9	0.80
ECLIF2/ND-MAX SAJF 1	17.64	31.3	89.3	1.20	133.9	0.80
ECLIF2/ND-MAX SAJF 2	17.64	31.34	89.6	1.20	134.4	0.80
ECLIF2/ND-MAX SAJF 3	17.64	31.17	88.4	1.20	132.6	0.80
ECLIF2/ND-MAX HEFA (JS-B2)	17.64	31.66	91.7	1.20	137.5	0.80
airegEM Ref	17.64	31.2	88.6	1.20	132.9	0.80
airegEM ReadiJet™ (JS-B3)	17.64	31.1	87.7	1.20	131.5	0.80
airegEM ATJ (JS-B1)	17.64	31.7	92.1	1.19	138.2	0.80
ATJ-SKA	17.64	31.5	90.4	1.20	135.7	0.80
SIP (Farnesane)	17.64	31.6	91.2	1.20	136.8	0.80
FT-Light	17.64	31.7	92.0	1.19	138.0	0.80
DEMO-SPK Ref A/C	17.64	31.08	87.8	1.20	131.7	0.80
DEMO-SPK Ref Lab	17.64	31.13	88.1	1.20	132.2	0.80
DEMO-SPK MB A/C	17.64	31.27	89.1	1.20	133.6	0.80
DEMO-SPK MB SIP	17.64	31.2	88.7	1.20	133.0	0.80
JETSCREEN JS-A1	17.64	31.16	88.4	1.20	132.6	0.80
JETSCREEN JS-A1.3	17.64	31.31	89.4	1.20	134.0	0.80
JETSCREEN JS-B1	17.64	31.62	91.4	1.20	137.1	0.80
JETSCREEN JS-C1	17.64	30.69	85.2	1.20	127.9	0.80
JETSCREEN JS-C3	17.64	31.0	87.6	1.20	131.3	0.80
NJFCP A1 (JP-8: POSF 10264)	17.64	31.3	89.2	1.20	133.8	0.80
NJFCP A2 (Jet A: POSF 10325)	17.64	31.1	88.1	1.20	132.1	0.80
NJFCP A3 (JP 5: POSF 10289)	17.64	31.0	87.3	1.20	130.9	0.80
ACCESS2 Reference	17.64	31.1	87.9	1.20	131.8	0.80
ACCESS2 HEFA Blend (50:50)	17.64	31.4	90.0	1.19	135.0	0.80
Neste Jet A-1 Ref	17.64	31.3	89.0	1.20	133.5	0.80
Neste HFP HEFA Blend 1	17.64	31.3	89.5	1.19	134.2	0.80

Fuel	Ar [g/min]	Fuel [mg/min]	O_2 (Fuel-rich) [mg/min]	Φ	O_2 (Fuel-lean) [mg/min]	Φ
Neste HFP HEFA Blend 2	17.64	31.4	89.8	1.20	134.7	0.80
Neste HFP HEFA Neat	17.64	31.6	91.5	1.19	137.2	0.80

4. Results

In the following the emphasis is given on the description and interpretation on the experimental results for the 42 jet fuels. Phenomenological findings and relations with the complex fuel composition are presented and discussed. A deep analysis of the underling chemical reaction network is, however, beyond the scope of the present publication. The interested reader is referred to Part-II [42] and Part-III [43] of this series for further insights.

4.1 Fuel Decay and Major Species

The global reaction behavior of the 42 technical fuels, i.e. concentration profiles of the reactants and products, follows the expectations as drawn from single compound fuels [37, 44]. Figure 2 gives an example of the major species profile evolution for the multiblend containing conventional and three alternative fuel components (DEMO-SPK MB SIP) at lean conditions. At low reactor temperatures the reactants pass the reactor unaltered. With increasing temperature fuel decay and conversion into first combustion intermediates, e.g. formaldehyde (CH_2O) and butadiene (C_4H_6), can be observed (compare insert). Simultaneously, a slight consumption of oxygen as well as formation of hydrogen and carbon monoxide occurs. Evolution of the species pool towards smaller intermediates can be observed with increasing reactor temperature (not shown). At a certain temperature, rapid conversion is observed when radical producing chain branching reactions overshoot the chain termination reactions. A steep increase of the final products H_2O and CO_2 is observed with complete intermediate consumption. The reactor temperature can be interpreted as a kind of reaction progress variable. Due to the well-characterized temperature conditions in the reactor, detailed kinetic modeling is feasible and has been previously demonstrated for single species fuels, e.g. methane [38], ethylene glycol [45] or n-alkanes [44]. The detailed examination of the reaction network of the complex fuels considered here is possible based on the presented data and is presented in Part-III of the present

series [43]. The aim of this part is to analyze the differences observed in the intermediate species pool of this large set of fuels in the following.

The product profiles for water and carbon dioxide of all fuels are compared in Fig. 2. Intentionally, the final concentration of CO_2 is similar for all fuels, since the reaction conditions are designed to exhibit similar carbon flows. Once conversion is complete the CO_2 concentrations are identical for all fuels, as shown for the lean conditions presented. Additionally, the experimental accuracy can be read from the deviation of the measured values and is found to be well within 10%. Consistently, the H_2O concentration for a specific fuel depends on the hydrogen content of that fuel.

The temperature for full occurrence of conversion is of interest, and can be visualized by both species CO_2 and H_2O. All fuels that fulfill the ASTM specification requirements exhibit very similar profiles with a span of only 8K, which is below the temperature accuracy of the experiment (±10K). This observation indicates similar reaction properties, i.e. ignition delay time and flame speed, which is consistent with previous findings [19] and a key intention of the standardization of fuel properties. Noticeable differences only occur for fuels that are clearly outside the specification requirements, such as for the FT-crude (FT-Light) product (lowest temperature) and the ATJ (highest temperature). The FT-Light almost exclusively consists of n-alkanes, while the major constituent of the ATJ fuel are two highly branched alkanes containing tertiary carbons similar to iso-octane. The resulting tert-butyl radicals produced by the ATJ are inert compared to other hydrocarbon radicals and thus exhibits delayed ignition as known from the octane index for spark ignition engine fuels. Furthermore, it should be noted that the ATJ exhibits slightly staged profile shapes for H_2O and O_2 as observed for iso-octane [42]. The interested reader is referred to Part-II of this series for a detailed examination of the reaction network of linear and branched alkanes [42] including the present fuels.

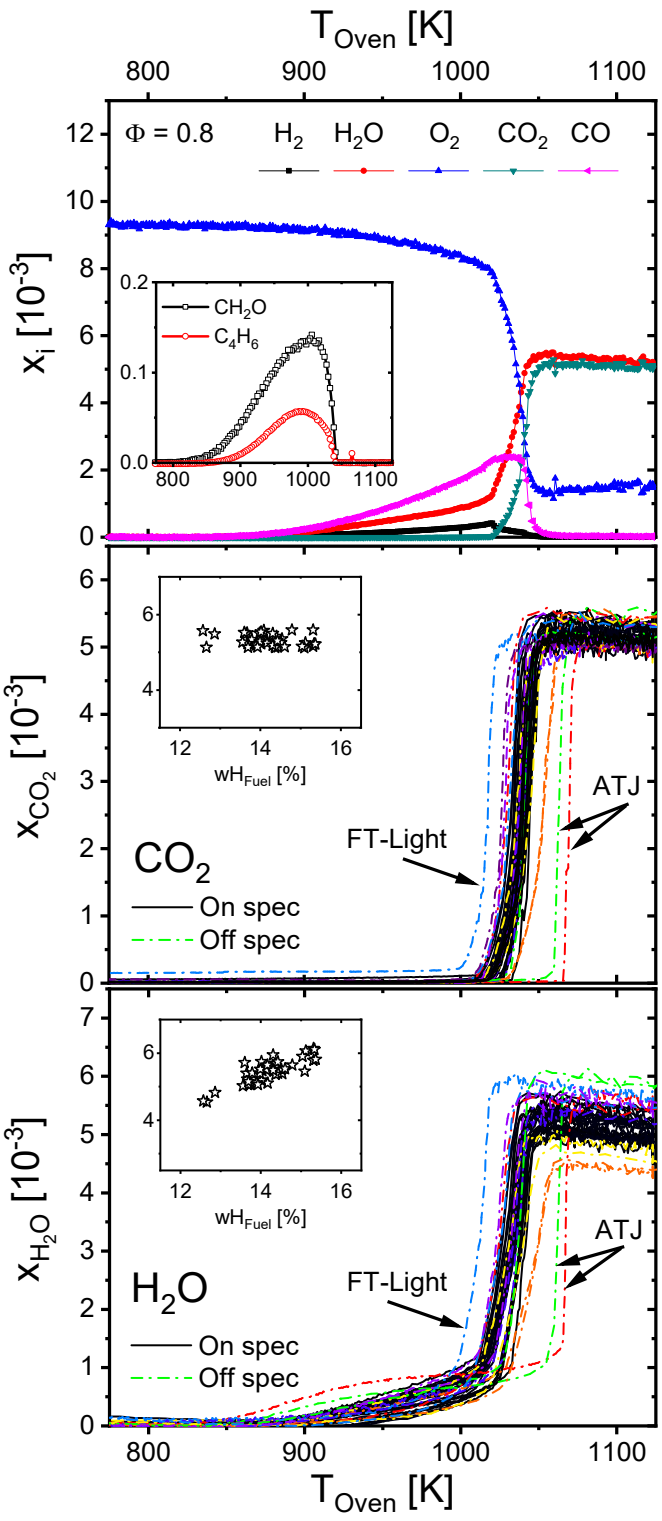

Figure 2: Major species and representative intermediates (CH_2O and C_4H_6) for the "Multiblend" kerosene containing HEFA, ATJ, SIP and conventional kerosene (panel 1). Comparison of carbon dioxide (panel 2) and water profiles (panel 3) for all fuels (Φ=0.8). Fuels outside the ASTM-D7566 specification are drawn in dashed lines. Inserts show the respective maximum values as function of the fuels' hydrogen content.

The present experiment allows for species resolved observation of the individual fuel molecules destruction during the oxidation reaction. The decay behavior depends in general more on the individual chemical classes than on the particular fuel. Since most of the fuels presented here are mixtures containing several hundreds of chemical species, a detailed quantitative determination is barely possible by the TOF-MBMS. When detailed fuel composition (see electronic supplement) is available then, the fuel profiles are calibrated accordingly. Figure 3 gives the species profiles by chemical class for the Jetscreen "JS A1" fuel as example, for comparison profiles are normalized to their respective maximum. Jetscreen "JS A1" represents a regular fossil Jet A-1 fuel exhibiting a composition close to the "world average" as determined in ref. [46]. Similar plots are given in the electronic supplement for each of the fuels.

As a rough generalization the decay order, i.e. the temperature at which a class starts to be consumed, can be stated in accordance to the thermal stability: n/iso-alkanes < cycloalkanes < mono-aromatics < di-aromatics. Additionally, a dependence on the chain length, i.e. carbon number, can be stated within some chemical classes. In particular only minor differences can be observed for the decay behavior of n- and iso-paraffins while a small shift towards lower decay temperatures can be stated for cyclic (mono- and di-) paraffins. Within in these classes some small species (e.g. C_8H_{16} or C_9H_{16}) are even formed in small amounts as intermediate by the chemical reactions prior beginning of their consumption. Classes containing aromatic structures (mono-, naphtheno- or diaromatics) in general show a distinct dependence on the respective chain length. Among these classes also typical combustion and soot precursor intermediates can be found. Indeed, a typical intermediate species profile is seen for the smaller molecules of the aromatic classes. The transition from "intermediate" to "fuel" profile shape occurs at C9 for monoaromatics, C11 for naphthenoaromatics and C12 for diaromatics. The occurrence of an intermediate species behavior is found to be highly dependent on the specie's initial concentration at the respective fuel. For example, $C_{10}H_{20}$ (cycloalkane), C_9H_{12} (monoaromatic) or $C_{11}H_{20}$ (bicycloalkane) exhibit fuel-shaped profiles in the JS-A1 fuel (Fig. 3), while intermediate-shaped profiles can be considered for $C_{10}H_{22}$ at ATJ (JS-B1), C_9H_{12} at S-IPK as well as $C_{11}H_{20}$ at HEFA (JS-B2). At the SIP (Farnesane) fuel, consisting of a single alkane, all of the

mentioned species exhibit intermediate shaped profiles. In all cases the fraction of the respective species is not detectable, or close to the detection limit at the fuel analysis. In general, the fuel decay profiles are found to be quite similar for all fuels as long as the respective class is a constituent of the fuel.

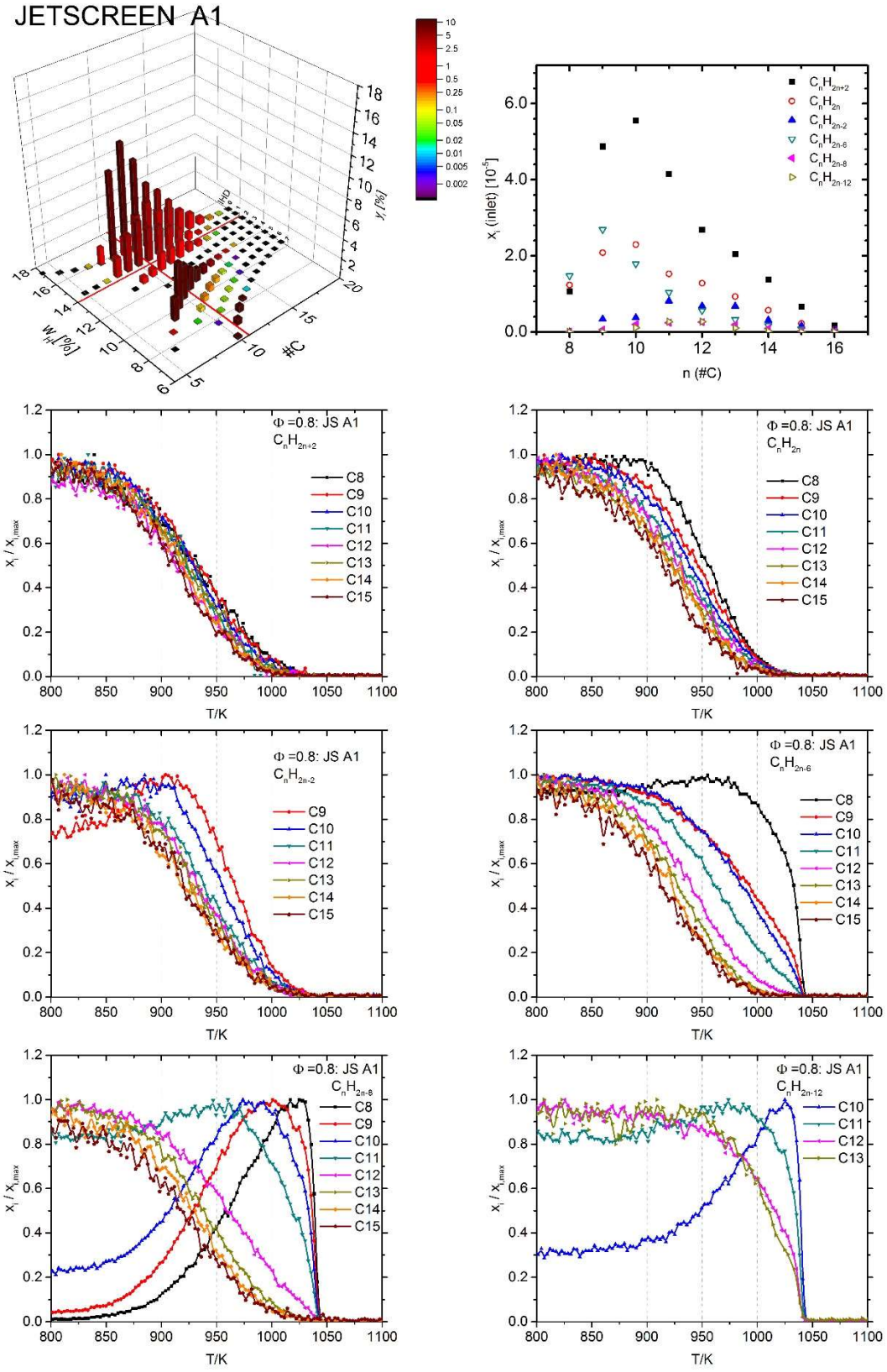

Figure 3: Fuel composition for Jetscreen JS A1 (top, left) and respective inlet mole fractions (top, right). Lower panels show the normalized fuel species profiles for the respective chemical class: n/iso-paraffins (CnH2n+2),

mono-cyclic paraffins (CnH2n), bicyclic paraffins (CnH2n-2), mono-cyclic aromatics (CnH2n-6), naphthenic-mono-aromatics (CnH2n-8), diaromatics (CnH2n-12).

4.2 Small Intermediate Species

In the following sections intermediate species concentrations are compared for the different fuels. Since the profile shapes and peak temperatures are quite similar, we will focus on the measured peak mole fractions only. Figure 4 summarizes some important combustion intermediates: ethylene (C_2H_4), propene (C_3H_6), butene (C_4H_8), and formaldehyde (CH_2O). Peak mole fractions are plotted against the fuel's hydrogen content since many combustion properties are linked to this fuel property. Ethylene as most other small combustion intermediates does not show a distinct relation with the fuel hydrogen content. Most fuels exhibit even similar peak concentrations ($x(C_2H_4) \sim 7.5 \cdot 10^{-6}$). It is noticeable that hydrogen-rich fuels depart significantly from the mean value. For these neat aliphatic fuels, a strong influence of the fuel structure is observed: the highest amount of C_2H_4 is seen for the n-alkane rich FT-Light fuel while the lowest is seen for the highly branched ATJ (major constituents: 2,2,4,6,6-pentamethyl heptane and 2,2,4,4,6,8,8-heptamethyl nonane).

The influence of the branching structure of alkanes can also be stated for propene (C_3H_6). Here the slightly branched farnesane exhibits the highest concentration. This finding agrees well with the decomposition pathways of this molecule [37] that provides many pathways towards propene and other C3-intermendiates. The FT crude fuel (FT-Light) and HEFA exhibit a mean value, and ATJ again shows a relatively low mole fraction. In contrast to C_2H_4 a slight increase of the C_3H_6 peak concentrations can be stated with increasing hydrogen content of the fuel. The butene (C_4H_8) peak maxima exhibit a similar dependence as propene on the hydrogen content in general. In addition, the divergence between the fuels is higher for the aliphatic fuels. For butene a clear dependence on the molecular structure is seen for the hydrogen rich i.e. alkane rich fuels. Values are additionally plotted versus n/iso-alkane ratio of the fuel. Highest values are seen for ATJ followed by a commercial SPK (SASOL IPK) and farnesane (SIP), all of which do not contain any n-alkanes. In combination, the amount and branching ratios of the alkanes dominate the C_4H_8 peak mole fraction. It should be noted

that no separation of 1-, 2- and isobutene was obtained here, and the split between these isomers will also be highly dependent on the fuel structure and also may influence the accuracy of the measured peak mole fractions. Oxygenated intermediates, formaldehyde (CH_2O) for instance, show only a slight dependence on the fuel hydrogen content but no distinct relation to the molecular fuel structure can be drawn.

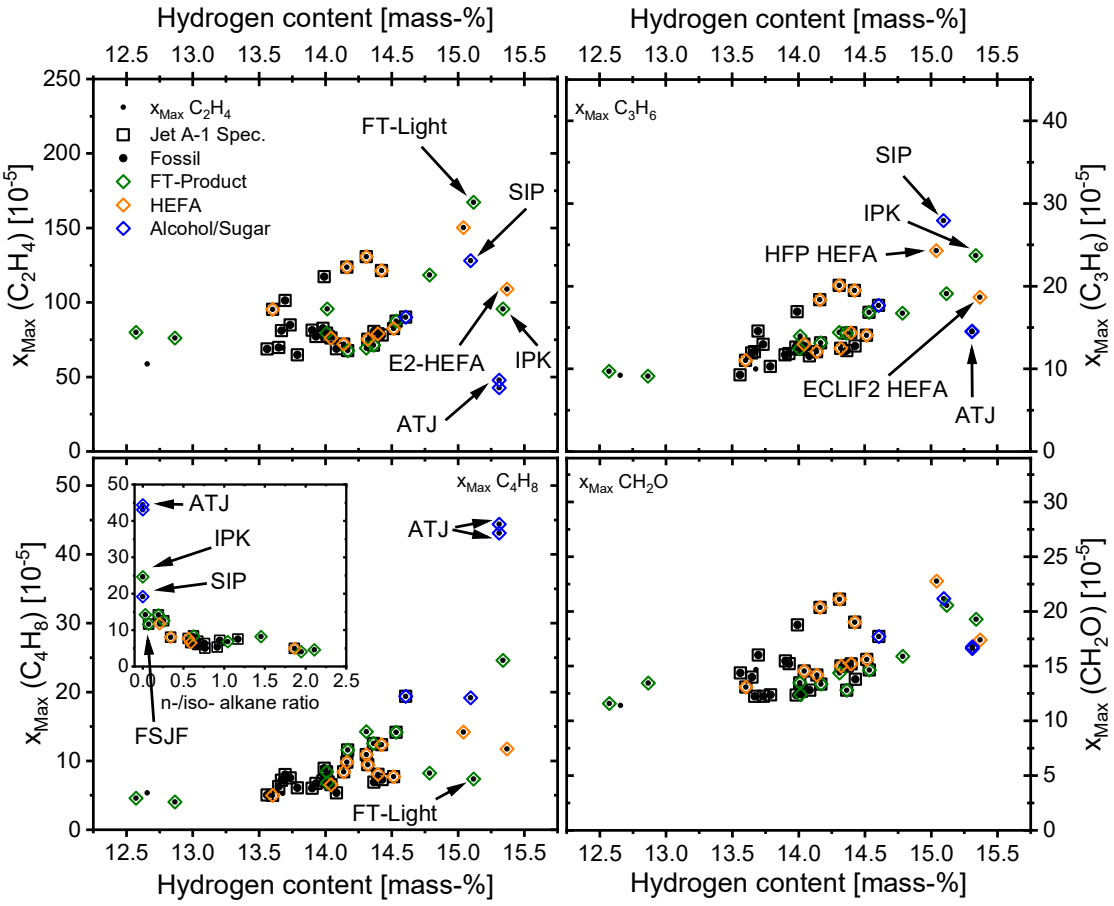

Figure 4: Peak mole fraction (Φ=0.8) of the combustion intermediates ethylene (C_2H_4), propylene (C_3H6), butene (C_4H_8) and formaldehyde (CH_2O) as a function of the fuel hydrogen content and n-/iso alkane ratio (insert). Fuels fulfilling ASTM-D7566 requirements are highlighted by black squares, colors indicate the respective group according Tab. 1.

4.3 Soot Precursor

Soot emission of aero-engines was found to correlate with the aromatic content or the hydrogen content of the fuel, e.g. [4, 10, 26]. Often both properties are used synonymously since aromatics constitutionally exhibit lower hydrogen content than aliphatic species. However, most recent work

proves the hydrogen content being a better indicator [5, 10]. From single compound fuels it is known that the sooting tendency of the chemical classes present in technical jet fuels roughly increase in the following order: n-alkanes < iso-alkanes < cycloalkanes (naphthenes) << mono-aromatics < di-aromatics [47]. The hydrogen content enables to account for the different structural features to a certain extent. Furthermore, the molecule size is also considered since aliphatic substituents will increase the hydrogen content of a molecule. Compare benzene (w_H=7.7mass-%) vs. dipropyl benzene (w_H=11.2mass-%) for instance. Both molecules exhibit a single aromatic ring and would count equally to the aromatics content of the fuel. In the following we further modify this approach and use the Index of Hydrogen Deficiency (IHD) [48] of the respective fuel. The IHD accounts for the amount of unsaturation in, i.e. number of double bound equivalents of a molecule. Alkenes or cycloalkanes for instance exhibit an IHD of one since they have one H_2 unit less than their respective alkane. An aromatic ring consequently yields an IHD of four. For a complex hydrocarbon fuel (C_xH_y) the IHD is derived according to Eq. 1 based on hydrogen mass fraction (w_H) and mean molar mass (M_{Fuel}):

$$IHD\left(C_xH_y\right) = (x+1) - \frac{y}{2} = \frac{\bar{M}_{Fuel}(1-w_H)}{M_C} - \frac{w_H\,\bar{M}_{Fuel}}{2M_H} + 1 \qquad \text{(Eq.1)}$$

Equation 1 shows that the IHD scales linearly with the hydrogen content when the molecule size does not change significantly. Technical fuels, in particular those within the jet fuel specification exhibit a quite similar molar mass. However, the IHD gives the advantage to enable comparison even with fuels of a wider range and will set the pure aliphatic compounds to zero. In Fig. 5 the peak mole fractions of important soot precursor intermediates such as benzene (C_6H_6), indene (C_9H_8), naphthalene ($C_{10}H_8$), and phenanthrene/anthracene ($C_{14}H_{10}$) are shown. These soot precursors show a convincing correlation with the IHD. For benzene the linear regression would give a line through origin, while the higher soot precursors show a slight shift to larger IHDs with a similar slope. This finding is true for all other detected aromatic soot precursor intermediates here. Since the molecular mass of the investigated fuels is in a narrow range, a similar conclusion can also be drawn for the hydrogen content (not shown).

In general, the fuels containing alternative components exhibit lower soot precursor concentrations compared to fossil fuels and support the soot reducing properties reported in many field experiments [25, 26]. Following the expectations, aliphatic fuels (IHD~0) exhibit the lowest concentrations in soot precursors. For the larger soot precursors (naphthalene and above) they are even close or below the detection limit and appear to be negligible compared to other fuels. Only for the aromatic free fuels a dependency of the soot precursors with fuel's iso-alkane content can be drawn [43]. The heavily branched ATJ exhibits the highest benzene concentration followed by the SASOL-IPK, HEFA and farnesane (SIP) and the lowest concentration is seen for the n-alkane rich FT-Light. This FT-crude product also has a noticeable alkene content shifting the IHD above zero. However, the alkene content seems not to influence the soot precursor chemistry significantly in this case. The measured peak mole fraction is comparable to neat decane [24].

The largest amount of soot precursor species was found for the hydrogen-lean FT-product streams and the academic surrogates. Namely SASOL-LD#2, SASOL-HN#2 and Jetscreen surrogate JS-C1. None of these fuels are covered by the ASTM standard, but are of high interest for this systematic consideration. While SASOL-LD#2 follows the extrapolated trend of certified fuels, SASOL-HN#2 and JS-C1 fall below this trend when mono aromatic soot precursor species are considered (i.e. benzene). This can be potentially linked to an extraordinary content of multi-ring naphthenic (di- and tri- cycloalkanes) species in these fuels. The hydrotreated Jetscreen A1.3 also exhibits an increase benzene concentration. This behavior could be attributed to the hydrogenation of diaromatics towards bicyclic naphthene's [49].

Interestingly the SASOL-HN#2 achieves its IHD by a high amount of mono-aromatic species while the JS-C1 does by di-aromatics. JS-C1 consequently overshoots the trend of naphthalene while smaller aromatics are formed in subpar amount. SASOL-LD#2 exhibits a balanced mixture and consequently follows the trend. The disproportionately high levels of indene (C_9H_8) for the fuels HN#1, HN#2 and JS-B3 (ReadiJet) can be linked to the noticeable amounts of indane (C_9H_{10}) content

of the fuels. It is further noticeable that the differences between the highly unsaturated fuels vanish when higher soot precursor species are considered.

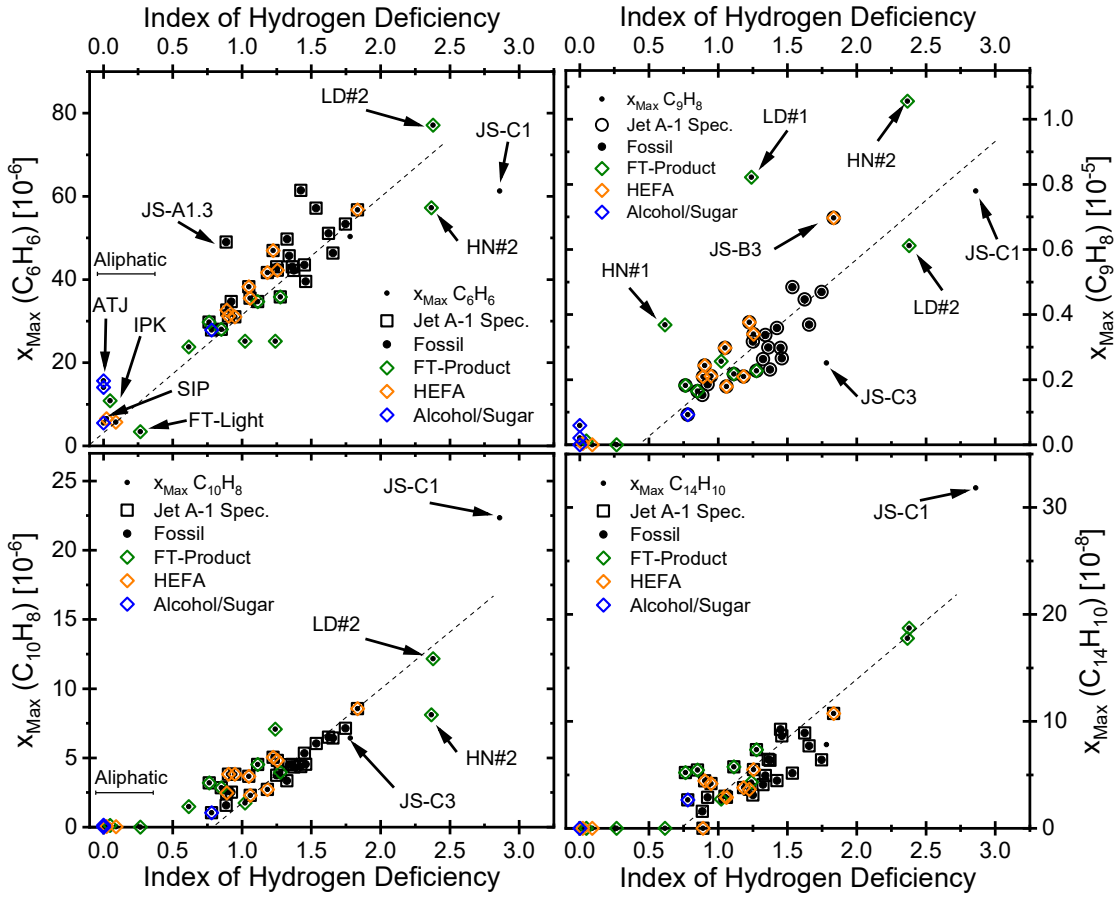

Figure 5: Peak mole fractions (Φ=1.2) of the soot precursor intermediates benzene (C_6H_6), indene (C_9H_8), naphthalene ($C_{10}H_8$), and phenanthrene/anthracene ($C_{14}H_{10}$) as a function of the degree of unsaturation expressed in IHD. Fuels fulfilling ASTM requirements are highlighted by black squares, colors indicate the respective group according table 1. Lines are drawn to guide the eye.

The amount of di-aromatics (naphthalenes) is often correlated to the sooting tendency of a technical fuel. To a certain extent the IHD or hydrogen content also covers the naphthalene content of the fuel, since multi-ring aromatics have a higher IHD or lower hydrogen content. Indeed, an influence of the naphthalene content beyond the IHD cannot be drawn for small soot precursors. However, when multi-ring aromatics are considered, a noticeable correlation can be verified. Figure 6 gives the peak mole fractions of phenanthrene/anthracene ($C_{14}H_{10}$), fluorene ($C_{13}H_{10}$), naphthalene ($C_{10}H_8$) and indane (C_9H_8) as a function of the naphthalene content of the fuel. It should be noted that the applied

naphthalene test (ASTM-D1840) measures the mass fraction of the sum of all di-aromatic species based on an assumed absorption cross section typical for conventional mineral oil products. The peak mole fractions of $C_{14}H_{10}$ clearly rise with increasing naphthalene content within fuels of similar IHD (same color). Additionally, the level of this gain increases within increasing IHD as shown in Fig. 6. A similar behavior can be stated for $C_{13}H_{10}$. For SASOL-LD#2 a remarkably high $C_{13}H_{10}$ concentration was measured while at the same time indene is relatively low. This might be linked to the significant amount of tricyclic-paraffins contained in this fuel. For $C_{10}H_8$ and smaller soot precursor intermediates (e.g. C_9H_8) no distinct correlation to the naphthalene content can be seen. The detected concentration rises only by the increase of IHD as visualized in Fig. 5.

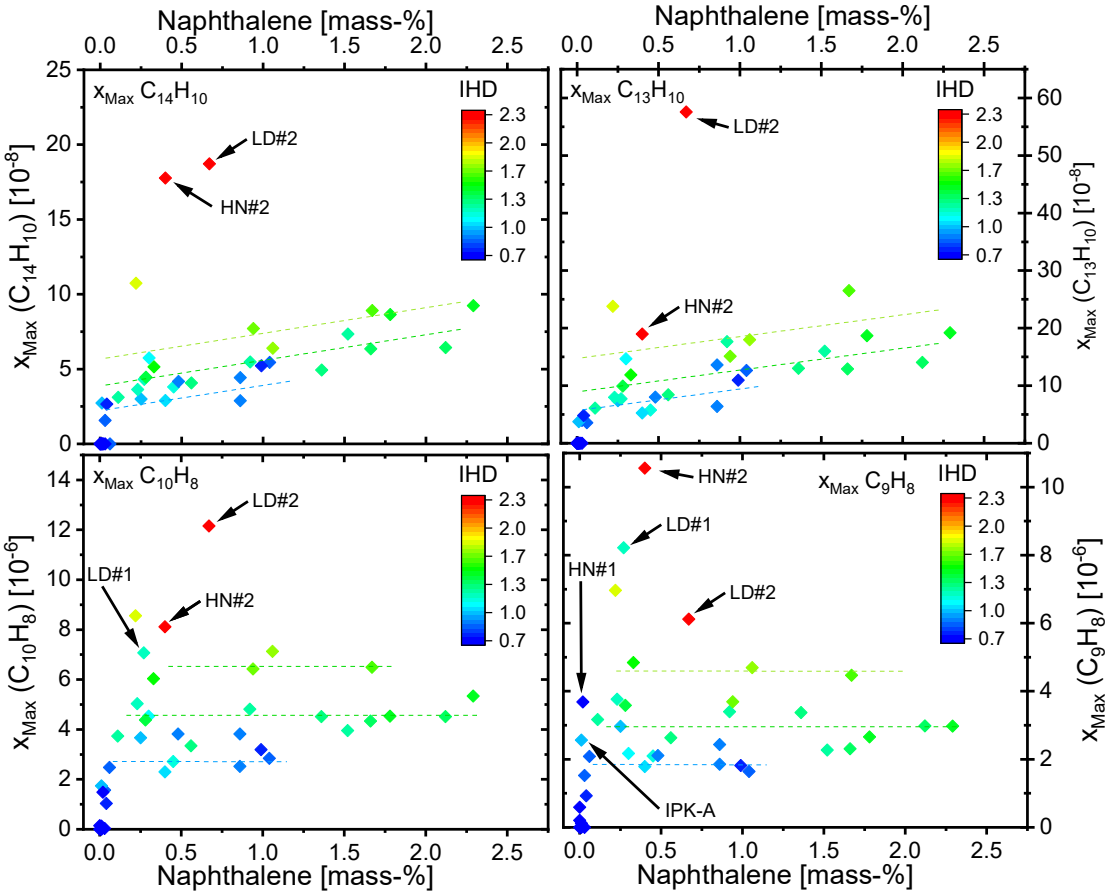

Figure 6: Peak mole fractions (Φ=1.2) of poly-aromatic soot precursor species $C_{14}H_{10}$, $C_{13}H_{10}$, $C_{10}H_8$ and C_9H_8 as function of the naphthalene content (ASTM-D1840) the IHD (Index of Hydrogen Deficiency) of the respective fuel is color-coded. Lines are drawn to guide the eye.

5. Summary

Part-I of our trilogy on alternative aviation fuels covers the experimental framework for the subsequent modeling approach. A respective collection on over 40 technical fuel samples is presented and characterized here providing the basis for experimental and modeling work of this trilogy.

Detailed examination is provided by measurements at the DLR high-temperature flow reactor. Fuels are selected from numerous national and international large-scale projects, which can be linked to a large number of complementary experiments like engine or inflight emission measurements. Quantitative evolution of combustion reaction intermediates is recorded for slightly rich (Φ=1.2) and lean (Φ=0.8) conditions. This unique dataset provides systematic insights on the influence of the chemical composition on the combustion kinetics of chemically complex fuels and is available for further model development. Readers are encouraged to get in contact with the authors for additional results obtained within this series.

The general reaction behavior was found to be almost identical when fuels fulfill the current specification. Also fuel decay was observed to be widely independent from the fuel composition and the consumption of different chemical classes are similar in most fuels but each class shows an individual decomposition behavior. The influence of the chemical composition of the fuel on the intermediate species pool was examined. The structure of alkanes (e.g. branched vs. linear) as major constituent of most fuels, was seen to dominate the intermediate species pool solely when no other chemical classes are present.

Special attention was given to the soot precursor chemistry of the fuels. A general systematic dependency of the soot precursor concentration on the degree of unsaturation IHD (Index of Hydrogen Deficiency) or the hydrogen content respectively, was demonstrated. Beyond this, additional increases of larger soot precursor species with the fuels' naphthalene (di-aromatic) content were shown. To the best of our knowledge this is the first time that this relationship was systematically proven for complex technical fuels on a molecular level. This will be covered in Part-II

[42] from a modeling point of view with the presentation of the elaborate surrogate modeling approach, followed by the application on technical fuels presented here in Part-III [43] of this series.

Acknowledgements

Tim Edwards for providing the NJFCP fuels and Marc Mühlberg for his experimental contributions are gratefully acknowledged. DLR has received funding from the European Union's Horizon 2020 research and innovation program under grant agreement No 723525 (JETSCREEN). Don't Panic!

References

[1] Wang M, Dewil R, Maniatis K, Wheeldon J, Tan T, Baeyens J, et al. Biomass-derived aviation fuels: Challenges and perspective. Prog Energy Combust Sci 2019;74:31-49. https://doi.org/10.1016/j.pecs.2019.04.004

[2] Drünert S, Neuling U, Zitscher T, Kaltschmitt M. Power-to-Liquid fuels for aviation – Processes, resources and supply potential under German conditions. Applied Energy 2020;277. https://doi.org/10.1016/j.apenergy.2020.115578

[3] Doliente SS, Narayan A, Tapia JFD, Samsatli NJ, Zhao Y, Samsatli S. Bio-aviation Fuel: A Comprehensive Review and Analysis of the Supply Chain Components. Frontiers in Energy Research 2020;8. https://doi.org/10.3389/fenrg.2020.00110

[4] Lobo P, Hagen DE, Whitefield PD. Comparison of PM emissions from a commercial jet engine burning conventional, biomass, and Fischer-Tropsch fuels. Environ Sci Technol 2011;45(24):10744-9. https://doi.org/10.1021/es201902e

[5] Brem BT, Durdina L, Siegerist F, Beyerle P, Bruderer K, Rindlisbacher T, et al. Effects of Fuel Aromatic Content on Nonvolatile Particulate Emissions of an In-Production Aircraft Gas Turbine. Environ Sci Technol 2015;49(22):13149-57. https://doi.org/10.1021/acs.est.5b04167

[6] Moore RH, Thornhill KL, Weinzierl B, Sauer D, D'Ascoli E, Kim J, et al. Biofuel blending reduces particle emissions from aircraft engines at cruise conditions. Nature 2017;543(7645):411-5. https://doi.org/10.1038/nature21420

[7] Kleine J, Voigt C, Sauer D, Schlager H, Scheibe M, Jurkat-Witschas T, et al. In Situ Observations of Ice Particle Losses in a Young Persistent Contrail. Geophys Res Lett 2018;45(24):13,553-13,61. https://doi.org/10.1029/2018gl079390

[8] Moore RH, Shook MA, Ziemba LD, DiGangi JP, Winstead EL, Rauch B, et al. Take-off engine particle emission indices for in-service aircraft at Los Angeles International Airport. Sci Data 2017;4:170198. https://doi.org/10.1038/sdata.2017.198

[9] Speth RL, Rojo C, Malina R, Barrett SRH. Black carbon emissions reductions from combustion of alternative jet fuels. Atmos Environ 2015;105:37-42. https://doi.org/10.1016/j.atmosenv.2015.01.040

[10] Schripp T, Anderson B, Crosbie EC, Moore RH, Herrmann F, Osswald P, et al. Impact of Alternative Jet Fuels on Engine Exhaust Composition During the 2015 ECLIF Ground-Based Measurements Campaign. Environ Sci Technol 2018;52(8):4969-78. https://doi.org/10.1021/acs.est.7b06244

[11] Christie S, Lobo P, Lee D, Raper D. Gas Turbine Engine Nonvolatile Particulate Matter Mass Emissions: Correlation with Smoke Number for Conventional and Alternative Fuel Blends. Environ Sci Technol 2017;51(2):988-96. https://doi.org/10.1021/acs.est.6b03766

[12] Curran HJ. Developing detailed chemical kinetic mechanisms for fuel combustion. Proc Combust Inst 2018. https://doi.org/10.1016/j.proci.2018.06.054

[13] Wang H, Xu R, Wang K, Bowman CT, Hanson RK, Davidson DF, et al. A physics-based approach to modeling real-fuel combustion chemistry - I. Evidence from experiments, and thermodynamic, chemical kinetic and statistical considerations. Combust Flame 2018;193:502-19. https://doi.org/10.1016/j.combustflame.2018.03.019

[14] Xu R, Wang K, Banerjee S, Shao J, Parise T, Zhu Y, et al. A physics-based approach to modeling real-fuel combustion chemistry – II. Reaction kinetic models of jet and rocket fuels. Combust Flame 2018;193:520-37. https://doi.org/10.1016/j.combustflame.2018.03.021

[15] Won SH, Haas FM, Dooley S, Edwards T, Dryer FL. Reconstruction of chemical structure of real fuel by surrogate formulation based upon combustion property targets. Combust Flame 2017;183:39-49. https://doi.org/10.1016/j.combustflame.2017.04.032

[16] Abdul Jameel AG, Naser N, Issayev G, Touitou J, Ghosh MK, Emwas A-H, et al. A minimalist functional group (MFG) approach for surrogate fuel formulation. Combust Flame 2018;192:250-71. https://doi.org/10.1016/j.combustflame.2018.01.036

[17] Haylett DR, Davidson DF, Hanson RK. Ignition delay times of low-vapor-pressure fuels measured using an aerosol shock tube. Combust Flame 2012;159(2):552-61. https://doi.org/10.1016/j.combustflame.2011.08.021
[18] Ji C, Wang YL, Egolfopoulos FN. Flame Studies of Conventional and Alternative Jet Fuels. J Propul Power 2011;27(4):856-63. https://doi.org/10.2514/1.B34105
[19] Richter S, Braun-Unkhoff M, Naumann C, Riedel U. Paths to alternative fuels for aviation. CEAS Aeronaut J 2018;9(3):389-403. https://doi.org/10.1007/s13272-018-0296-1
[20] Dagaut P, Cathonnet M. The ignition, oxidation, and combustion of kerosene: A review of experimental and kinetic modeling. Prog Energy Combust Sci 2006;32(1):48-92. https://doi.org/10.1016/j.pecs.2005.10.003
[21] Dagaut P, Diévart P. Combustion of synthetic jet fuels: Naphthenic cut and blend with a gas-to-liquid (GtL) jet fuel. Proceedings of the Combustion Institute 2017;36(1):433-40. https://doi.org/10.1016/j.proci.2016.05.045
[22] Dooley S, Won SH, Chaos M, Heyne J, Ju Y, Dryer FL, et al. A jet fuel surrogate formulated by real fuel properties. Combust Flame 2010;157(12):2333–9. https://doi.org/10.1016/j.combustflame.2010.07.001
[23] Oßwald P, Köhler M. An atmospheric pressure high-temperature laminar flow reactor for investigation of combustion and related gas phase reaction systems. Rev Sci Instrum 2015;86(10):105109. https://doi.org/10.1063/1.4932608
[24] Jürgens S, Oßwald P, Selinsek M, Piermartini P, Schwab J, Pfeifer P, et al. Assessment of combustion properties of non-hydroprocessed Fischer-Tropsch fuels for aviation. Fuel Process Technol 2019;193:232-43. https://doi.org/10.1016/j.fuproc.2019.05.015
[25] Moore RH, Shook M, Beyersdorf A, Corr C, Herndon S, Knighton WB, et al. Influence of Jet Fuel Composition on Aircraft Engine Emissions: A Synthesis of Aerosol Emissions Data from the NASA APEX, AAFEX, and ACCESS Missions. Energy Fuels 2015;29(4):2591-600. https://doi.org/10.1021/ef502618w
[26] Schripp T, Herrmann F, Oßwald P, Köhler M, Zschocke A, Weigelt D, et al. Particle emissions of two unblended alternative jet fuels in a full scale jet engine. Fuel 2019;256:115903. https://doi.org/10.1016/j.fuel.2019.115903
[27] Won SH, Dooley S, Veloo PS, Wang H, Oehlschlaeger MA, Dryer FL, et al. The combustion properties of 2,6,10-trimethyl dodecane and a chemical functional group analysis. Combust Flame 2014;161(3):826-34. https://doi.org/10.1016/j.combustflame.2013.08.010
[28] Richter S, Kathrotia T, Naumann C, Kick T, Slavinskaya N, Braun-Unkhoff M, et al. Experimental and modeling study of farnesane. Fuel 2018;215:22-9. https://doi.org/10.1016/j.fuel.2017.10.117
[29] Zschocke A, Scheuermann S, Ortner J. High biofuel blends in aviation (HBBA). 2012. https://doi.org/S0016-2361(19)31255-4/h0080
[30] Schripp T, Grein T, Zinsmeister J, Oßwald P, Köhler M, Müller-Langer F, et al. Technical application of a ternary alternative jet fuel blend – Chemical characterization and impact on jet engine particle emission. Fuel 2020;in Press. https://doi.org/10.1016/j.fuel.2020.119606
[31] Edwards JT. Reference Jet Fuels for Combustion Testing. 55th AIAA Aerospace Sciences Meeting. 2017.
[32] Bullerdiek N, Buse J, Dögnitz N, Feige A, Halling A-M, Hauschild S, et al. Einsatz von Multiblend-JET-A-1 in der Praxis, DEMO-SPK finar report (in German). BMVI; 2019.
[33] Rauch B, al. e. JET Fuel SCREENing and Optimization https://cordis.europa.eu/project/id/723525. 2020.
[34] Riazi MR. Lee-Kesler Method from Characterization and Properties of Petroleum Fractions. ASTM International; 2005.
[35] Herrmann F, Jochim B, Oßwald P, Cai L, Pitsch H, Kohse-Höinghaus K. Experimental and numerical low-temperature oxidation study of ethanol and dimethyl ether. Combust Flame 2014;161(2):384-97. https://doi.org/10.1016/j.combustflame.2013.09.014
[36] Köhler M, Oßwald P, Xu H-B, Kathrotia T, Hasse C, Riedel U. Speciation data for fuel-rich methane oxy-combustion and reforming under prototypical partial oxidation conditions. Chem Eng Sci 2016;139:249-60. https://doi.org/10.1016/j.ces.2015.09.033

[37] Oßwald P, Whitside R, Schäffer J, Köhler M. An experimental flow reactor study of the combustion kinetics of terpenoid jet fuel compounds: Farnesane, p-menthane and p-cymene. Fuel 2017;187:43-50. https://doi.org/10.1016/j.fuel.2016.09.035
[38] Chu TC, Buras ZJ, Oßwald P, Liu M, Goldman MJ, Green WH. Modeling of aromatics formation in fuel-rich methane oxy-combustion with an automatically generated pressure-dependent mechanism. Phys Chem Chem Phys 2019;21(2):813-32. https://doi.org/10.1039/c8cp06097e
[39] Biordi JC. Molecular beam mass spectrometry for studying the fundamental chemistry of flames. Prog Energy Combust Sci 1977;3(3):151-73. https://doi.org/10.1016/0360-1285(77)90002-8
[40] Oßwald P, Hemberger P, Bierkandt T, Akyildiz E, Köhler M, Bodi A, et al. In situ flame chemistry tracing by imaging photoelectron photoion coincidence spectroscopy. Rev Sci Instrum 2014;85(2):025101. https://doi.org/10.1063/1.4861175
[41] Krüger D, Oßwald P, Köhler M, Hemberger P, Bierkandt T, Karakaya Y, et al. Hydrogen abstraction ratios: A systematic iPEPICO spectroscopic investigation in laminar flames. Combust Flame 2018;191:343-52. https://doi.org/10.1016/j.combustflame.2017.12.025
[42] Kathrotia T, Oßwald P, Naumann C, Richter S, Köhler M. Combustion Kinetics of Alternative Jet Fuels, Part-II: Reaction Model for Fuel Surrogate. Manuscript submitted to Fuel 2020.
[43] Kathrotia T, Oßwald P, Zinsmeister J, Methling T, Köhler M. Combustion Kinetics of Alternative Jet Fuels, Part-III: Fuel Modeling and Surrogate Strategy. Manuscript submitted to Fuel 2020.
[44] Kathrotia T, Oßwald P, Köhler M, Slavinskaya N, Riedel U. Experimental and mechanistic investigation of benzene formation during atmospheric pressure flow reactor oxidation of n-hexane, n-nonane, and n-dodecane below 1200 K. Combust Flame 2018;194:426-38. https://doi.org/10.1016/j.combustflame.2018.05.027
[45] Kathrotia T, Naumann C, Oßwald P, Köhler M, Riedel U. Kinetics of Ethylene Glycol: The first validated reaction scheme and first measurements of ignition delay times and speciation data. Combust Flame 2017;179:172-84. https://doi.org/10.1016/j.combustflame.2017.01.018
[46] Hadaller OJ, Johnson JM. CRC Report No. 647: World Fuel Sampling Program. CRC Aviation Fuel, Lubricant & Equipment Research Committee of the Coordinating Research Council, Inc; 2006.
[47] Minchin ST. Luminous Stationary Flames: the Quantitative Relationship between Flame Dimensions at the Sooting Point and Chemical Composition, with Special Reference to Petroleum Hydrocarbons. J Inst Petr Techn 1931;17:S. 102-20.
[48] Kathrotia T, Riedel U. Predicting the soot emission tendency of real fuels – A relative assessment based on an empirical formula. Fuel 2020;261:116482. https://doi.org/10.1016/j.fuel.2019.116482
[49] Pelucchi M, Oßwald P, Pejpichestakul W, Frassoldati A, Mehl M. On the combustion and sooting behavior of standard and hydro-treated jet fuels: An experimental and modeling study on the compositional effects. Proc Combust Inst 2020. https://doi.org/10.1016/j.proci.2020.06.353